N.A-TM DRA/MARSHALL

IFAORS

Institute For Atmospheric Optics And Remote Sensing

Office: 101 Research Drive, Hampton, VA 23666 Telephone: (804) 865-0811
Mailing: P.O. Box P, Hampton, VA 23666

F-520

July 20, 1984

N84-31837

National Aeronautics and Space Administration
George C. Marshall Space Flight Center
Alabama 35812

Contract: NAS8-35594

Subject: Monthly Progress Report--Development of a Global Model for Atmospheric Backscatter at CO_2 Wavelengths

Period: June 14 - July 13, 1984

Attn: Dr. D. E. Fitzjarrald (ED42)
Technical Monitor, NAS8-35594

Introduction

Work has been carried out on the tasks shown below.

Task 1.1: To examine experimentally measured size distributions for the free troposphere, fit bimodal log-normal models with different refractive indices for the two modes and calculate β_{CO_2}

A program has been written which fits a bimodal log-normal model to an aerosol size distribution for which dN/d(log r) is specified at six values of the radius, r. An iterative technique is used to converge onto the final solution. The program outputs dN/d(log r) for each log-normal independently, as well as the log-normal constants N, r_g and σ_g. An example of its application to simulated data is shown in Fig. 1, where the experimental points are shown by round dots, the individual fitted curves by dashed lines and the total fitted bimodal distribution by the solid line.

During the coming month, this program will be applied to real data and the range of log-normal parameters examined. These will be used to generate scattering cross-sections at 10.6 μm, as well as conversion factors for 1 μm extinction to 10.6 μm backscatter.

Task 1.2: To investigate the effect of aerosol microphysical processes occurring in an aerosol plume which undergoes transport in the atmosphere, on its β_{CO_2} value

The 10 layer model, which has been used to study the effect of gravitational sedimentation on aerosol particle size distribution, has been expanded by incorporating the transport effect due to vertical diffusion.

Vertical diffusion processes have been employed widely in 1-D models for studying the vertical distributions of atmospheric gases, as well as of aerosol particles (see, for example, Toon et al., JAS, 36, 718-736, 1979). For small aerosol particles, this can be an important transport mechanism. For large particles, the gravitational sedimentation is perhaps the dominant transport processes. For simplicity, the same diffusion coefficient is applied to all sizes of particles. The vertical flux of aerosol particles, due to diffusion, can be written as

$$\phi = D\, n_a \frac{\partial}{\partial z}\left(\frac{n_p}{n_a}\right) \qquad (1)$$

where n refers to the concentration, and a and p denote the air molecule and aerosol particle, respectively. D is the diffusion coefficient. Since the diffusion flux depends on the gradient of aerosol particle concentration, the diffusion processes tend to smooth out the vertical aerosol distributions. Figures 1 to 3 show model results. The diffusion coefficient used in these computations is 3×10^4 cm^2/sec. Calculations have also been made by using the coefficient of Toon et al., which is one order of magnitude greater than the one just mentioned. We have found that this coefficient leads to relatively much faster changes in vertical aerosol distributions with time.

Figure 2 shows the time variation of aerosol particle concentration. Only the results for every other time step are shown in the figure. They are denoted sequentially by ●, ■, ♦, ▲, ◣, and ◣. The time increment in the numerical calculation is set to be one-tenth of a day. This time step seems to be an adequate choice as revealed in the model results. It should be mentioned that the model used in the analysis includes not only the diffusion processes, but also the effect due to aerosol coagulation and gravitational sedimentation. Comparing Fig. 2 with the results of earlier analyses we have conducted, it is found that vertical diffusions affect aerosol distribution more effectively than coagulation or sedimentation processes. The distinct features in Fig. 2 are the increase of aerosol particles between altitudes of 4 and 6 km and the reduction of particle concentration in the dust layer (from 1 to 4 km). In the bottom layer, the particle concentration shows also a slight increase. The increase in particle concentration of the two layers just above the dust layer is solely due to vertical diffusion processes. This result illustrates the smoothing effect of the diffusion on the profiles of aerosol distributions. As anticipated and shown in Fig. 2, the majority of the aerosol particles in the dust layer are removed from the atmosphere by gravitation sedimentation processes. The time change of the particle mode radius is given in Fig. 3. A shifting of the model radius to larger values is found in the layers immediately above and below the dust layer. This is primarily due to the incoming of larger particles from the dust layer. Within the dust layer, the model radius shows a

decrease in values. This feature can be the reduction of large particles due to largely sedimentation processes. Figure 4 shows the time change of σ. In the layers above the dust layer, σ exhibits a decrease in value, while an increase of σ is found in the lowest three layers.

Task 2.1: <u>Use of the SAGE/SAM II Data Set</u>

Work has continued on the study of the SAGE/SAM II data. The following has been accomplished.

All SAGE data (33 months) and one year of SAM II data has been processed. Approximately one year of the data has been examined in detail. This data shows clearly the north-south latitudinal variation discussed in previous reports. It also shows a clear seasonal cycle. The period of greatest tropospheric aerosol concentration in both hemispheres is Spring-Summer, lower concentrations being observed in Fall-Winter. Dependence of aerosol concentration upon surface type is less clear. Only a study of the complete 33 months data set will establish whether there is, on the average, a significant difference between the free tropospheric aerosol over land and ocean.

Further work has been done on the extinction probability distributions. It is now believed that this reflects a genuine characteristic of the aerosol population at different altitudes, probably reflecting micro-physical changes produced by either temperature or humidity variations.

Task 2.2: <u>Analysis of the GAMETAG Data Set</u>

Good progress has been made on the analysis of the GAMETAG data set. Flight data for 1978 has been examined and backscatter and extinction values at 10.6 μm have been calculated using an aerosol model of mixed composition. Aerosols within the accumulation mode have been assigned the refractive index for ammonium sulphate, those within the coarse particle mode have been assigned a refractive index appropriate to soil particles. A particular study is being made of the fluctuations in backscatter cross-sections along the flight path of the measurements, using integration times of 1 minute and 5 minutes.

<u>Research Schedule for Next Month</u>

1. To continue work on the bi-modal aerosol model described under Task 1.1.

2. To continue work on the multi-layer numerical model described under Task 1.2.

3. To continue work on the SAGE/SAM II data set, in particular, the whole data set will be examined for confirmation of seasonal and latitudinal characteristics and for evidence of surface type influence.

4. To continue analysis of the GAMETAG data set under Task 2.2.

Remarks

No problems encountered.

G. S. Kent

G. S. Kent

cc: Code AP29-F
AS24D
AT01
EM13A-41
DCAS
ED42
NASA Scientific &
Technical Information Facility

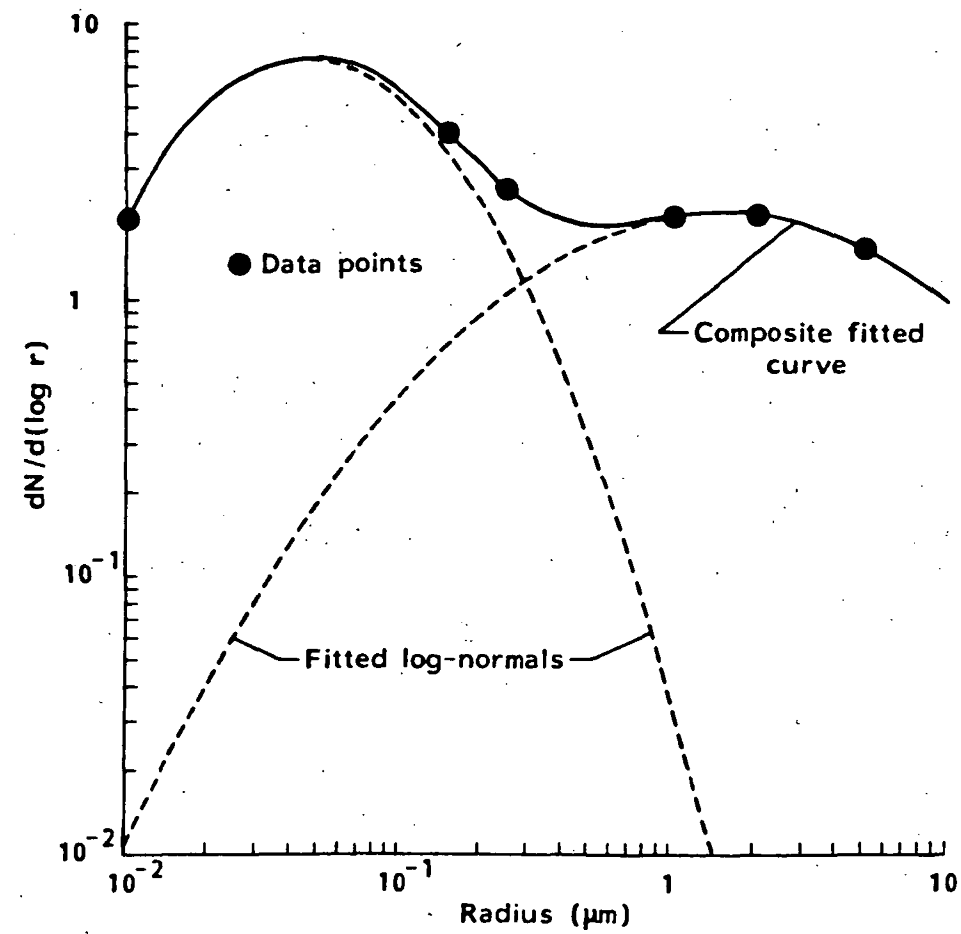

Fig. 1. Example of the application of the bi-modal log-normal fitting program to a simulated experimental size distribution.

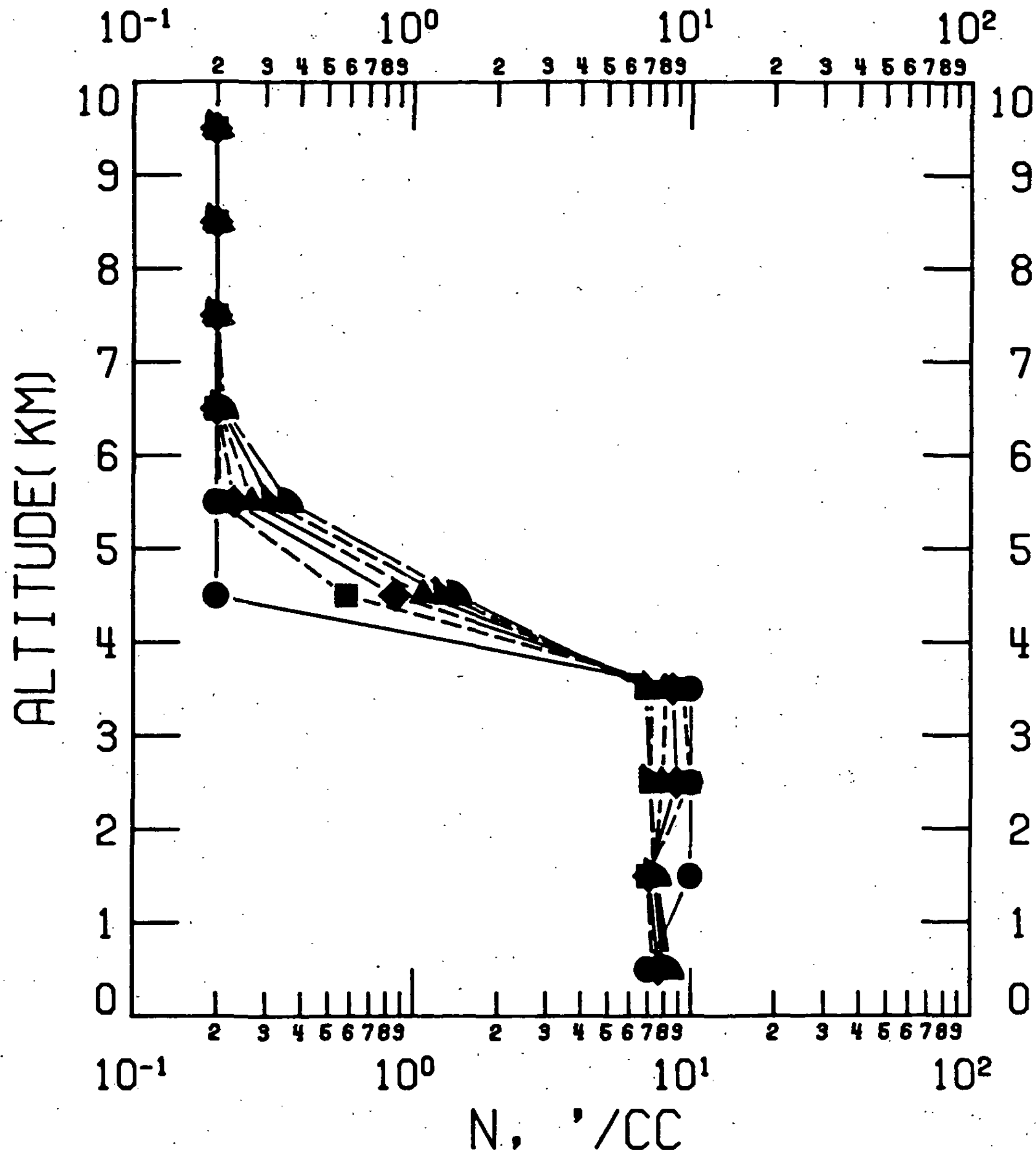

Fig. 2. Time variation of aerosol particle concentration (#/cc). The results of every other time step are denoted sequentially by ● (initial), ■, ◆, ▲, ◣, and ◗. The time increment is equal to one-tenth of a day.

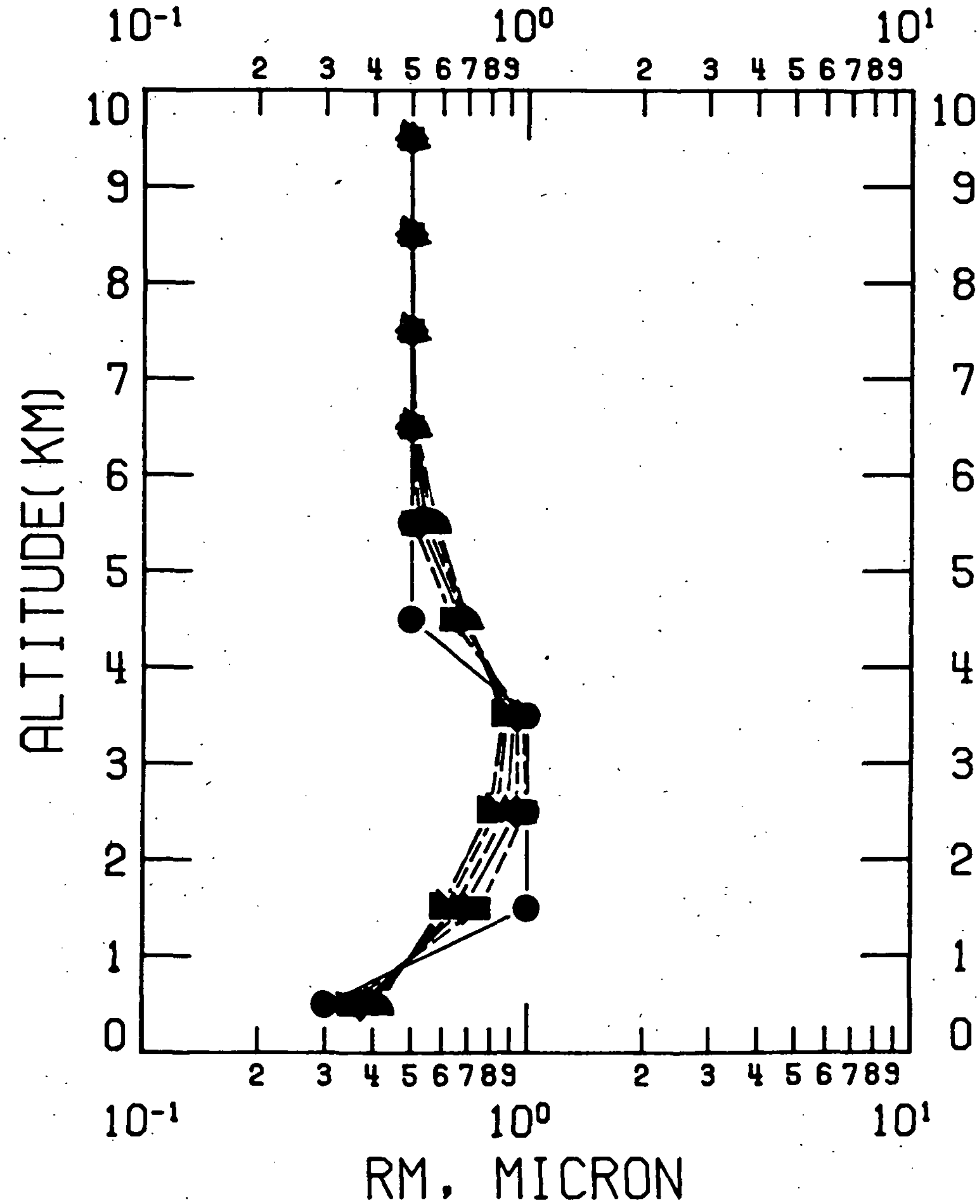

Fig. 3. The same as Fig. 2, except for mode radius r_m(μm).

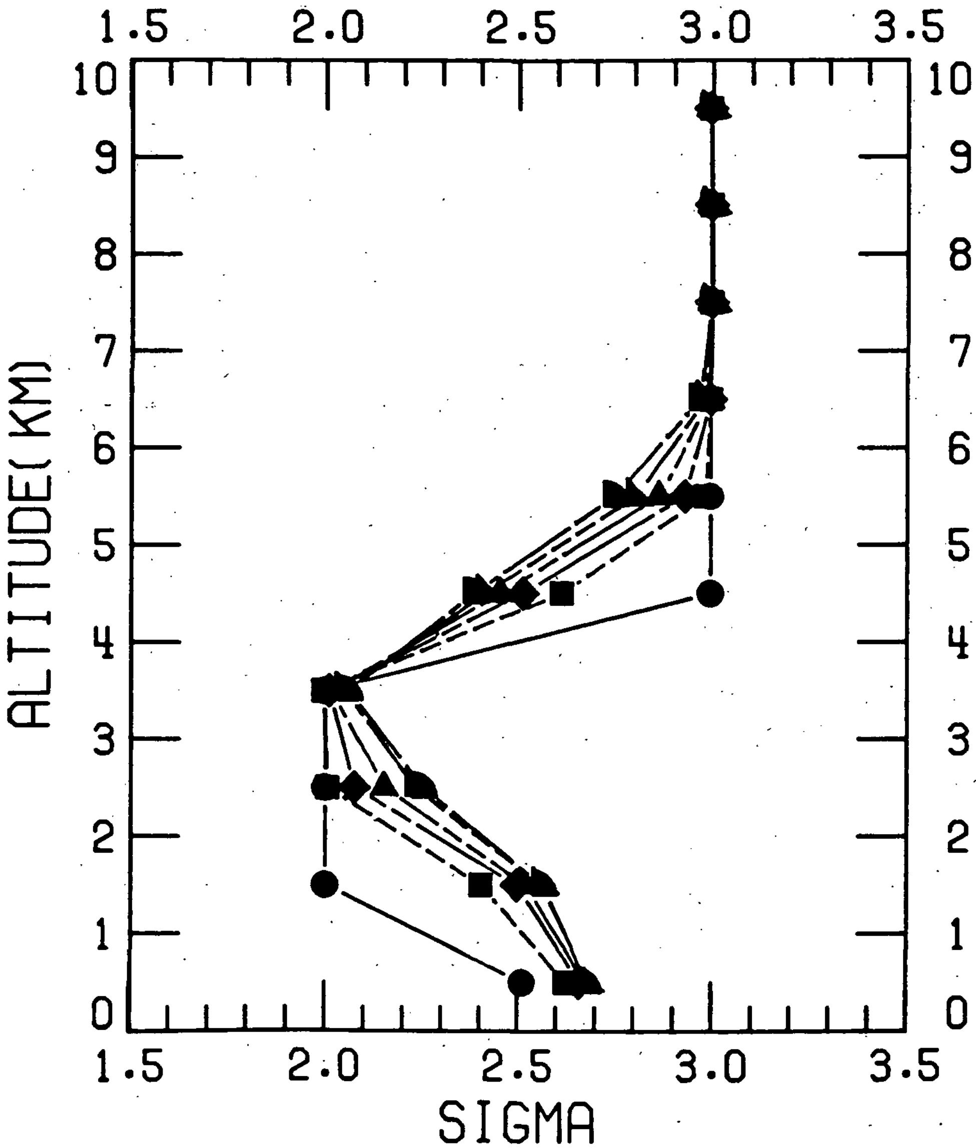

Fig. 4. The same as Fig. 2, except for geometric standard deviation ∂.